70th International Astronautical Congress (IAC), Washington, USA, 21-25 October 2019.

IAC-19-B4.IP.4

Writing with Sunlight: CubeSat Formation Control Using Aerodynamic Forces

Danil Ivanov[a], Shamil Biktimirov[b], Kirill Chernov[c], Alexander Kharlan[d], Uliana Monakhova[e], Dmitry Pritykin[f]*

[a] *Keldysh Institute of Applied Mathematics, RAS, Miusskaya sq.4, Moscow, Russian Federation, 125047,* danilivanovs@gmail.com
[b]*Skolkovo Institute of Science and Technology, Bolshoy Boulevard 30, bld. 1, Moscow, Russia 121205,* shamil.biktimirov@skolkovotech.ru
[c] *Moscow Institute of Physics and Technology, Institutsky lane 9, Moscow Region, Russia 141701,* chernow.kirill@gmail.com
[d]*Skolkovo Institute of Science and Technology, Bolshoy Boulevard 30, bld. 1, Moscow, Russia 121205,* aleksandr.kharlan@skoltech.ru
[e] *Keldysh Institute of Applied Mathematics, RAS, Miusskaya sq.4, Moscow, Russian Federation, 125047,* monakhova@phystech.edu
[f] *Skolkovo Institute of Science and Technology, Bolshoy Boulevard 30, bld. 1, Moscow, Russia 121205,* d.pritykin@skoltech.ru
* Corresponding Author

Abstract

The paper is devoted to the study of decentralized control with the use of differential lift and drag for constructing satellite formation flying in the shape of a required configuration. Each satellite in the formation is equipped with a sunlight reflector. In the appropriate lighting conditions such formation can be visible from Earth and provide graphic images in the sky. The paper studies the possibility of achieving a defined image configuration of the formation by decentralized aerodynamic-based control implemented via the sunlight reflectors' attitude relative to upcoming airflow.

1. Introduction

Small satellite formation missions have long been considered for various important applications where a large number of satellites serve as distributed instruments for atmospheric sampling, construct a distributed antenna platform, make a distributed aperture for imaging, etc. We study the design and evolution through time of small satellite formations comprising a number of spacecraft equipped with drag sails, that can be employed as sunlight reflectors. In the appropriate lighting conditions such formations, given the right attitude of the sails' reflecting surfaces, can be visible from Earth and provide graphic images in the sky. The formations can thus function as space media broadcasting logos or messages.

Preliminary feasibility studies [16] showed that such formations can be deployed using 12U CubeSats with $2x2m^2$ sails under suitable lighting conditions in a Sun-synchronous orbit. The minimum distance between two reflectors should be greater than 600m to be discernible by the human eye. If the attitude of the image is fixed in the orbital reference frame, it requires continuous control by onboard thrusters and leads to excessive fuel consumption. Another approach is to have the image rotating in the orbital reference frame with an orbital period. Each satellite can be appointed such initial conditions that it moves along a circumference in the orbital reference frame, so that each "pixel" in the image rotates with the same angular velocity without control according to the orbital dynamics. However, the control is required to achieve the relative trajectories.

The paper studies the possibility of achieving a defined image configuration of the formation by decentralized aerodynamic-based control. Each satellite is assumed to be equipped with an attitude control system. It allows changing the cross-section area and the attitude of the reflector relative to the incoming airflow, so the differential drag and lift forces appear. The satellites have an onboard navigation system and exchange information on the relative motion via an inter-satellite communication link. The required attitude is calculated for each satellite according to the difference between the actual and required relative motion. The final attitude of the reflectors and the attitude of the image satisfies the observability requirements.

The control approach based on the differential drag force was firstly proposed in 1980s by Leonard [1] under the assumption of a discrete change in the effective cross section of satellites flying in the group. He developed a control algorithm based on the proportional-differential controller. A large number of papers showed application of a variety of the different control algorithms using differential drag: PID controller [2], linear-quadratic regulator [3], Lyapunov-based control [4,5], sliding mode control [6], optimal

control [7] etc. However almost all these studies consider only two satellites in formation flying with application of the centralized control approach. A few papers are devoted to differential drag control of the multiple satellites. The cyclic and optimal control strategies for a cluster flight with more than two satellites are proposed in the paper [8]. Stability and performance of cluster keeping while avoiding collisions are studied in [9].

These papers considered only the aerodynamic differential drag application. Some recent papers take into account the differential lift as well. The application of the differential lift along with the drag for the small satellites rendezvous problem was first proposed by Horsley et. al. in [10]. Authors used the aerodynamic drag and lift forces model based on Sentman's treatment in the free molecular flow conditions [11]. Control strategy developed in [10] is based on the bang-bang approach when only the maximum values of the lift and drag are used. Paper [12] investigates some practical aspects of the trajectories proposed by Horsey et.al. and the collision risks during the rendezvous. The same model of the differential lift and drag is used in [13,14] where the neural-network-based sliding-mode adaptive controllers are proposed. Paper [15] addresses the problem of the satellite formation keeping by the differential lift and drag under the J_2 perturbation. In the papers cited above the lift force is perpendicular to the satellite velocity vector. The drag and lift coefficients depend on a set of atmosphere parameters and satellite attitude according to the used model. Here the simplified model of the aerodynamic force is used. The specific attitude is calculated with the goal to provide the required force in the end.

2. Preliminary study

Our preliminary study [16] was focused on designing a mission of CubeSats, equipped with reflectors and coordinated in a formation to produce in the sky a graphical image, which is seen from a given point of interest (POI) on Earth. The formation is deployed in LEO and the sunlight reflecting surfaces act simultaneously as solar sails and drag augmentation devices, and therefore can be employed to control the relative positions of satellites in the formation.

It is important to introduce a formal understanding of what is understood by "visibility". In theory, human eye can distinguish a star with a magnitude of 6 in the clear sky at night. Adding a few geometrical considerations, we define visibility by the set of conditions below:

- (1) the satellite should be in the direct line of vision from the POI;
- (2) the satellite should be lit by the Sun in order to be able to reflect the light to the ground;
- (3) the Sun must be below some established low elevation as seen from the POI. In this work, the limit is set to 5 degrees of elevation;
- (4) the spacecraft must be in the darker part of the sky when it passes, so the angle between the directions from the POI to the Sun, on one hand, and the satellite on the other, should not be less than a certain value, which was in this case set to 25 degrees;
- (5) the pixels must be clearly visible for the naked eye, and the message should be readable. In this work, this is defined by requiring the magnitude of -8.0 or better (the magnitude of the well known Iridium satellite flares varies between -8.0 and -9.5).

For a mission where it is required that the satellite appears above a given point on the ground at given times, it is essential to make sure that the orbit is such that the satellite is indeed observable and visible. The set of mission requirements and assumptions leave us with a narrow set of points in time and orbital position where the demonstration is possible. Thus the chosen strategy was to align the orbit with the terminator line (or make the orbit cross the terminator line over the POI if there is there is just one such point). In the case of multiple POIs, if the orbit remains in accordance with the terminator, the amount of views is more stable and easily controlled by selecting the correct LTAN. As the terminator line moves in the inertial frame in accordance with the Sun, the orbit of interest is, of course, a Sun-synchronous one (SSO).

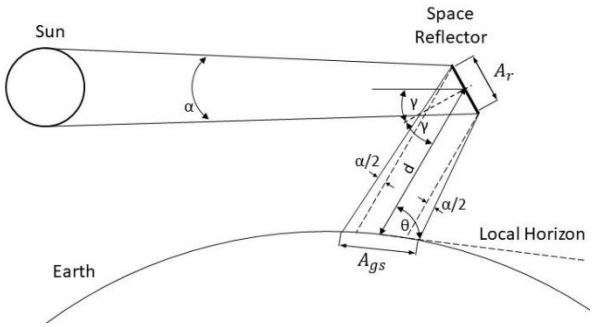

Fig.1. The reference frame associated with the point O moving along the circular orbit

For payload design let us consider a single satellite with a large sunlight reflector orbiting the Earth (Fig. 1). The scattering angle α is the included angle of the Sun measured from the Earth, d is the distance between reflector and ground spot, A_r and A_{gs} are the areas of the CubeSat reflector and the ground spot respectively.

The magnitude of the reflector is usually calculated as the ratio of incident light intensity to a reference intensity:

$$m = -2.5\log(I / I_{ref}),$$

The intensity of the light at the POI is given by:

$$I = I_0 A_r \rho\tau \cos\gamma \sin\theta \Big/ 4d^2 \tan^2\frac{\alpha}{2},$$

where $I_0 = 1360$ W/m^2 is the average intensity of solar energy at the Earth distance, ρ is the mirror reflectivity coefficient, γ is the incident angle of solar rays, θ is the elevation angle of the satellite; τ is the atmospheric transmissivity:

$$\tau = 0.1283 + 0.7559e^{-0.3878\sec(\pi-\theta)}.$$

Thin Mylar film coated with aluminum is chosen as the reflector material because of low weight and high reflectivity coefficient $(\rho = 0.92)$. Mylar solar sails have been tested in space missions. The reflector, which is deployed and maintained by a rigid support structure, is assumed to be of square shape.

Let us now estimate the size of the reflector necessary to ensure the required magnitude. Given light intensity and orbit altitude, one can express the reflector area A_r as a function of angles θ and γ. The extreme values of these two angles (yielding the maximum A_r) are $\theta_{\min} \approx 30^\circ$ (see conditions 3 and 4) and $\gamma_{\max} \approx 60^\circ$ (see conditions 2 and 3). Hence, we obtain the characteristic linear size of the reflector in the range of 2-2.6 m for SSO altitudes of 600-800 km. Seeing the need to pack the solar sail material along with the supporting beams into the CubeSat structure along with all other necessary satellite subsystems (including attitude control and propulsion units), we come to choose the 12U as a suitable CubeSat size for the designed formation. The total mass of each CubeSat is estimated to be 18 kg.

Let us recall now that our task is to produce a pixel image, which means that the distances between any two CubeSats in the formation must be such that they are distinguished as independent pixels. Human eye resolution is known to be about two arc-minutes, which for the specified SSO altitudes yields the minimum distance between satellites in the formation ranging from 625 to 812 m. The quality of the image is still acceptable when the relative positions errors do not exceed 30 m, which is well within the range of on-board GPS-module position determination.

The study [16] was principally focused on maintaining a constant formation flying along the terminator, which certainly requires heavy use of propulsion. The attempts to use the differential drag control to decrease the use of fuel showed that any significant difference in the fuel consumption (if aided by the differential drag) can be achieved at very low orbits with altitudes within 300-400 km.

The study proposed in this paper aims at obtaining a formation without use of any kind of propulsion. Hence, the orbit altitude used in the subsequent simulations is chosen to be 350 km. Our test simulations showed that even for such low orbits in order to speed up the control algorithm's convergence it is required to have a larger reflector than what our parametric model [16] yields. Thus, we arrived at the reflector's size 4x4 m, which allows constructing the required formation in about 30 hours. Discarding propulsion also means that we cannot hope to maintain the constant geometry of the propulsion. Instead we will devise certain reference trajectories, in which all the satellites in the formation move, so that the image can be seen in the correct orientation just once per orbit. A natural point of interest for this study is Washington DC and the time of the image display corresponds to the IAC-19 report time.

3. The problem statement

The problem of the satellite formation deployment after their separation from the launcher is considered, i.e. achieving the defined relative trajectories is required when each satellite is moving to form a specific flat image. It is assumed that each satellite is aware of the relative motion of all other members of the group. This information can be obtained either via an inter-satellite link or using autonomous relative motion determination system (range finders, optical sensors, etc.).

Initially, the satellites move in accordance with the specified initial conditions after the launch from the dispenser. The launch of the satellites is carried out using a certain launch system (usually with the help of special springs), and the system has execution errors. In the absence of control, it leads to a gradual increase in the distances between the satellites. In this paper, we suppose a formation launched into LEO. It is assumed that each satellite is equipped with an attitude control system, for example, reaction wheels-based system. So, the satellites are able to be controlled by the aerodynamic force, which depends on the attitude of satellite relative to the incoming airflow. In the paper the 12U CubeSats equipped with 4x4m sunlight reflectors are considered.

The main goal of the work is development of such a decentralized control of satellites, which leads to the formation of a required configuration. Linear quadratic regulator (LQR)-based control is applied for the task. It is assumed that each satellite is controlled independently from the others in decentralized approach.

3.1 Controlled Motion Equations

Consider a simplified instance of a formation consisting of two satellites in near circular orbits. The general form of the equations of the relative motion of two satellites is too complex for analytical consideration, so the Hill-Clohessy-Wiltshire equations [17,18] are used. This model describes the relative motion of two satellites flying in the near circular orbits in the central gravitational field. The orbital reference frame is used, its origin (reference point) moves along the circular orbit of radius r_0 with the orbital angular velocity $\omega = \sqrt{\mu / r_0^3}$, where μ is the Earth gravitational parameter. Axis *Oz* is aligned along the vector from the center of the Earth to the reference point, *Oy* axis is directed along the normal to the orbital plane, *Ox* axis complements the reference frame to the right-handed one (Fig.2).

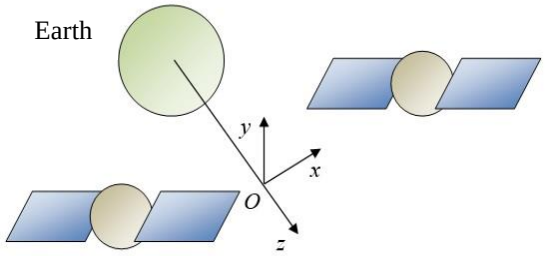

Fig.2. The reference frame associated with the point *O* moving along the circular orbit

Let $\mathbf{r}_i = (x_i, y_i, z_i)$ and $\mathbf{r}_j = (x_j, y_j, z_j)$ be the vectors of the conditional *i*-th and *j*-th satellites in the orbital reference frame, $i \neq j$, $i = 1,...,N$, $j = 1,...,N$, where N is the number of the satellites in the formation. Then the components of the relative position vector $\mathbf{r}_{ij} = \mathbf{r}_j - \mathbf{r}_i = (x_{ij}, y_{ij}, z_{ij})$ are governed by the following equations

$$\begin{cases} \ddot{x}_{ij} + 2\omega \dot{z}_{ij} = u_x^{ij}, \\ \ddot{y}_{ij} + \omega^2 y_{ij} = u_y^{ij}, \\ \ddot{z}_{ij} - 2\omega \dot{x}_{ij} - 3\omega^2 z_{ij} = u_z^{ij}, \end{cases} \quad (1)$$

where $\mathbf{u}_{ij} = \Delta\mathbf{f}_{ij} / m$, $\Delta\mathbf{f}_{ij} = \mathbf{f}_j - \mathbf{f}_i$ is the difference between the aerodynamic drag forces acting on the *i*-th and the *j*-th satellites, m is the mass of a satellite that is the same for all satellites in the group. In the case of free motion, i.e. if $\Delta\mathbf{f}_{ij} = 0$, the exact solution of (1) is

$$\begin{cases} x_{ij}(t) = -3C_1^{ij}\omega t + 2C_2^{ij}\cos(\omega t) - 2C_3^{ij}\sin(\omega t) + C_4^{ij}, \\ y_{ij}(t) = C_5^{ij}\sin(\omega t) + C_6^{ij}\cos(\omega t), \\ z_{ij}(t) = 2C_1^{ij} + C_2^{ij}\sin(\omega t) + C_3^{ij}\cos(\omega t), \end{cases}$$

where $C_1^{ij} - C_6^{ij}$ are constants that depend on the initial conditions at $t = 0$:

$$C_1^{ij} = \frac{\dot{x}_{ij}(0)}{\omega} + 2z_{ij}(0), C_2^{ij} = \frac{\dot{z}_{ij}(0)}{\omega}, C_3^{ij} = -3z_{ij}(0) - \frac{2\dot{x}_{ij}(0)}{\omega},$$

$$C_4^{ij} = x_{ij}(0) - \frac{2\dot{z}_{ij}(0)}{\omega}, C_5^{ij} = \frac{\dot{y}_{ij}(0)}{\omega}, C_6^{ij} = y_{ij}(0).$$

The term responsible for the relative drift is $-3C_1^{ij}\omega t$. Thus, the relative trajectory of two satellites is closed if and only if $C_1^{ij} = 0$. However, in practice such an ideal initial conditions for free motion cannot be specified, and in the case of perturbations and nonlinear effects there is always a relative drift between the satellites.

3.2 Aerodynamic Force Model

The physical processes of the interaction of the atmospheric particles with the satellite's surface are complex. However, one may construct a fairly simple model of these interactions using a limited number of empirical coefficients. Assume that the interaction proceeds mechanically through two schemes – a mirror one, when the reflection of the molecule from the surface is absolutely elastic, and diffuse one in the case of an absolutely inelastic collision. Define the actual reflection as a linear interpolation of these two interaction schemes, assuming that a certain part of the molecules ε are mirror-reflected, and the rest $(1-\varepsilon)$ part is reflected inelastically with the Maxwell distribution corresponding to the temperature T_r. In this case [19] the expression for the aerodynamic force acting on the reflector is

$$\mathbf{f}_i = -\frac{1}{m}\rho V^2 S\left\{(1-\varepsilon)(\mathbf{e}_V, \mathbf{n}_i)\mathbf{e}_V + 2\varepsilon(\mathbf{e}_V, \mathbf{n}_i)^2\mathbf{n}_i + (1-\varepsilon)\frac{\upsilon}{V}(\mathbf{e}_V, \mathbf{n}_i)\mathbf{n}_i\right\}. \quad (2)$$

In (2), ρ is the atmosphere density, m is the satellite mass, V is the airflow velocity, S is the reflector's area, $\mathbf{n}_i$ is the unit vector normal to the reflector, $\mathbf{e}_V$ is a unit vector directed along the velocity of the incoming airflow, $\upsilon = \sqrt{\pi R T_r / 2}$ is a parameter proportional to the most probable thermal velocity of the diffusely reflected molecules, R is the gas constant, $i = 1,...,N$. The first term in (2) determines the aerodynamic drag force directed against the velocity of the air flow. The second and the third terms, which define the lift force, are force components directed against the normal $\mathbf{n}_i$. In the aerodynamic force model (2) there are two interaction parameters, ε and $\eta = \upsilon / V$. Generally, they are not constant and depend on the angle of attack, the velocity of the incident particles and other characteristics of the flow and the surface. However, in this paper we consider some average values of the

parameters ε and η, and it is assumed that they are constant and do not depend on the attitude. In [19], the inverse problem was solved to determine these parameters using the flight data of the motion of the Proton satellites. According to these estimates the interaction schemes of the gas with the satellite surface in LEO are such that $\varepsilon \approx 0.1$ and $\eta \approx 0.1$. This force model is firstly used for formation flying control in [3].

Let us rewrite the expression for the force components (2) using angles θ and φ representing the normal vector to the reflector's surface (see Fig. 2)

$$\mathbf{n}_i = \begin{bmatrix} \sin\theta_i \\ \cos\theta_i \cos\varphi_i \\ \cos\theta_i \sin\varphi_i \end{bmatrix}.$$

The angle θ is chosen so that the aerodynamic force does not act on the satellite when $\theta = 0$. $\theta \in [0; \pi/2]$, if $\theta < 0$ then the other side of the reflector may be considered. Angle $\varphi \in [0, 2\pi)$.

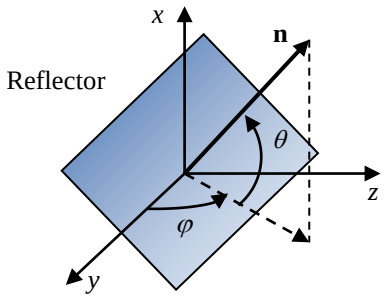

Fig.3. Angles defining the reflector's normal vector

The vector of incoming airflow is $\mathbf{e}_V = \begin{bmatrix} 1 & 0 & 0 \end{bmatrix}^T$ in the orbital reference frame. Substituting the values of $\mathbf{n}_i$ and $\mathbf{e}_V$ in the expression (2) of aerodynamic force,

$$\mathbf{f}_i = k \begin{bmatrix} -2\varepsilon(\sin\theta_i)^3 + \eta(\varepsilon-1)(\sin\theta_i)^2 + (\varepsilon-1)\sin\theta_i \\ -\cos\theta_i \sin\theta_i (\eta - \varepsilon\eta + 2\varepsilon\sin\theta_i)\cos\varphi_i \\ -\cos\theta_i \sin\theta_i (\eta - \varepsilon\eta + 2\varepsilon\sin\theta_i)\sin\varphi_i \end{bmatrix}$$

where $k = \frac{1}{m}\rho V^2 S$. Defining

$$p(\theta_i) = -2\varepsilon(\sin\theta_i)^3 + \eta(\varepsilon-1)(\sin\theta_i)^2 + (\varepsilon-1)\sin\theta_i,$$

$$g(\theta_i) = -\cos\theta_i \sin\theta_i (\eta - \varepsilon\eta + 2\varepsilon\sin\theta_i),$$

the expression for the aerodynamic force is simplified:

$$\mathbf{f}_i = k \begin{bmatrix} p(\theta_i) \\ g(\theta_i)\cos\varphi_i \\ g(\theta_i)\sin\varphi_i \end{bmatrix}. \qquad (3)$$

From (3), one can see that the *Ox* component of the aerodynamic force depends solely on the θ angle. The projection of the force on the plane *Oyz* is defined by the function $g(\theta_i)$ and its attitude is determined by the angle φ. The functions $p(\theta_i)$ and $g(\theta_i)$ are presented in Fig. 3 for $\varepsilon \approx 0.1$ and $\eta \approx 0.1$. The maximum value of f_x component of the aerodynamic force is achieved at $\theta = 90$ degrees (in the case when $p \approx 1.2$), i.e. when the reflector is perpendicular to the incoming airflow. The maximum projection of the force on the *Oyz* plane is smaller by an order of magnitude. It is about $g \approx 0.12$ at $\theta \approx 52$ deg. Besides at $\theta = 0$ and $\theta = 90$ deg. the function g equals zero. It means that the application of the force in the plane *Oyz* is possible only in the case of nonzero and non-maximal force along the axis *Ox*.

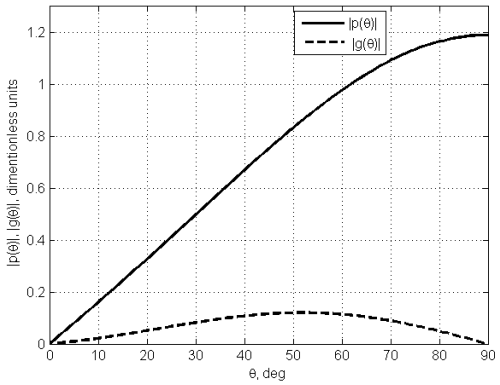

Fig.4. Components of the aerodynamic force with respect to angle θ

The paper considers the satellite relative motion control, so it is necessary to use the difference in the aerodynamic forces acting on two satellites,

$$\Delta\mathbf{f} = \mathbf{f}_1 - \mathbf{f}_2 = k \begin{bmatrix} p(\theta_1) - p(\theta_2) \\ g(\theta_1)\cos\varphi_1 - g(\theta_2)\cos\varphi_2 \\ g(\theta_1)\sin\varphi_1 - g(\theta_2)\sin\varphi_2 \end{bmatrix}. \qquad (4)$$

Thus, the differential aerodynamic force is defined by the four angles $\theta_1, \theta_2, \varphi_1, \varphi_2$. The value of the force projection on the plane *Oyz* is small as one can see from Fig. 3. So it better be maximized by setting $\varphi_2 = \varphi_1 + \pi$, i.e. the satellites rotate in opposite directions around *Ox* axis. In this case the value of Δf_{yz} component is defined by $g(\theta_1) + g(\theta_2)$,

$$\Delta\mathbf{f} = k \begin{bmatrix} p(\theta_1) - p(\theta_2) \\ (g(\theta_1) + g(\theta_2))\cos\varphi_1 \\ (g(\theta_1) + g(\theta_2))\sin\varphi_1 \end{bmatrix}. \qquad (5)$$

The maximum value of Δf_{yz} is twice the value of the projection of a single force in Fig.3. This is implied by the dependence of the differential aerodynamic force

$\Delta\mathbf{f}$ components on the angles θ_1 and θ_2 in Fig. 4. The acceptable control region in the dimensionless components of $\Delta\mathbf{f}$ is shown in Fig. 5. Since the attitude of the vector component Δf_{yz} in the plane *Oyz* is defined by the angle $\varphi_1 \in [0, 2\pi)$ it is necessary to rotate the area shown in Fig. 5 around the *Oy* axis to obtain the acceptable control region in three dimensions.

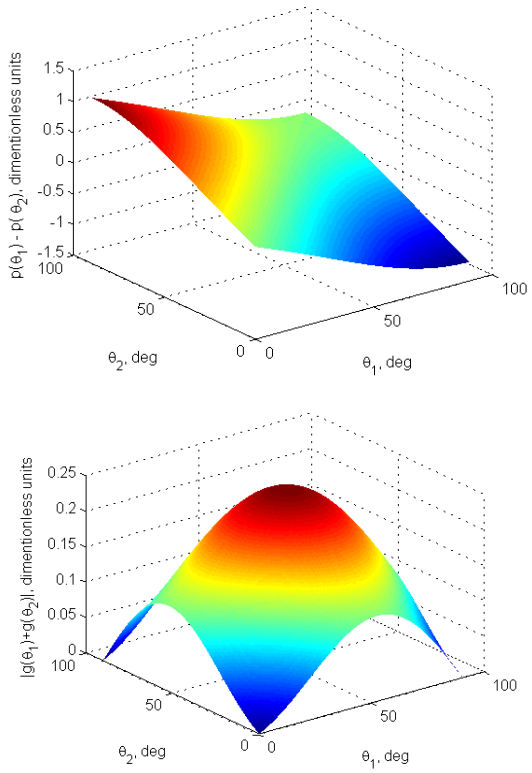

Fig.5. Functions $p(\theta_1) - p(\theta_2)$ and $|g(\theta_1) + g(\theta_2)|$

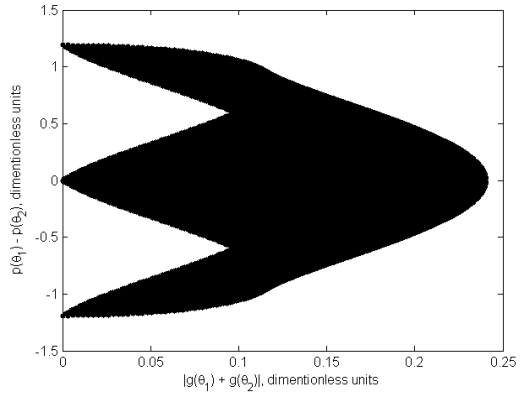

Fig.6. Acceptable control region

4. Control algorithm

Consider an application of the LQR regulator to track the predefined relative trajectory. This control algorithm is quite simple to implement in the case of two satellites in the group, but in the case of *N* satellites an additional decentralized control rule is needed. In this section an LQR is constructed and the decentralized approach is proposed.

4.1 LQR Construction

Rewrite (1) in the matrix-vector form

$$\dot{\mathbf{x}} = A\mathbf{x} + B\mathbf{u} \tag{6}$$

where $\mathbf{x} = [\mathbf{r}^T \ \mathbf{v}^T]^T$ is the state vector, A is the dynamic matrix

$A = \begin{bmatrix} 0_{3x3} & E \\ C & D \end{bmatrix}$, E is the identity matrix with size 3x3,

$C = \begin{bmatrix} 0 & 0 & 0 \\ 0 & -\omega^2 & 0 \\ 0 & 0 & 3\omega^2 \end{bmatrix}$, $D = \begin{bmatrix} 0 & 0 & -2\omega \\ 0 & 0 & 0 \\ 2\omega & 0 & 0 \end{bmatrix}$,

B is the control matrix

$B = \begin{bmatrix} 0_{3x3} \\ E \end{bmatrix}$,

$\mathbf{u} = \mathbf{u}_i - \mathbf{u}_j$ is the control vector. For a formation controlled by differential aerodynamic force the control vector $\mathbf{u} = \Delta\mathbf{f} / m$.

The desired relative motion corresponds to the free motion of the system described by the equation

$$\dot{\mathbf{x}}_d = A\mathbf{x}_d$$

where $\mathbf{x}_d$ is the desired state vector. Then one can obtain linear equation of the dynamics of the deviation from the desired trajectory

$$\dot{\mathbf{e}} = A\mathbf{e} + B\mathbf{u}, \tag{7}$$

where $\mathbf{e} = [\mathbf{x}^T - \mathbf{x}_d^T]^T$.

Linear quadratic regulator is the feedback control $\mathbf{u} = K\mathbf{e}$ which ensures the minimum of the functional

$$J = \int_0^\infty (\mathbf{e}^T Q\mathbf{e} + \mathbf{u}^T R\mathbf{u})dt \tag{8}$$

along the trajectory [20]. Here Q, R are the positive definite matrices that determine the weight of errors for the state vector and the weight of the control resource consumption respectively.

The feedback minimizing the functional is determined by the equation

$$\mathbf{u} = -R^{-1}B^T P\mathbf{e}, \tag{9}$$

where the matrix P is obtained as a solution of the Riccati equation

$$A^T P + PA - PBR^{-1}B^T P + Q = 0. \tag{10}$$

The Riccati equation (10) can be solved to obtain the matrix P if the weight matrices Q and R are known. Then the control vector $\mathbf{u}$ is calculated according to (9) using the current vector of the trajectory deviation $\mathbf{e}$. The matrices Q and R are the parameters of the algorithm. They characterize the transient processes. The problem is to choose such matrices Q and R that

they would ensure the required performance of the algorithm under the given control constraints.

4.2 Average deviation from the desired trajectories

The main problem of the LQR application to the multi-satellite formation is that for each of the *N* satellites there are *N-1* desired trajectories relative to each of the rest of the satellites. The desired relative trajectories are chosen in the way that all the satellites are located in the spots corresponding to the respective pixels of the letters-to-be-displayed during the motion. So, each satellite needs to apply the control (9) for each trajectory deviation. But the deviations $\mathbf{e}_{ij}$ could lead to the completely different control vectors $\mathbf{u}_{ij}$. That is why a strategy has to be defined for the constructing of the required formation.

We propose the following scheme to solve this problem. For each satellite one can calculate the mean vector of the deviations $\bar{\mathbf{e}}_i$ as follows:

$$\bar{\mathbf{e}}_i = \sum_{j=1}^{N-1} \mathbf{e}_{ij} / (N-1),$$

Then, using (9), the control vector is calculated:

$$\bar{\mathbf{u}}_i = -R^{-1} B^T P \bar{\mathbf{e}}_i . \qquad (11)$$

Thus, the relative trajectory of the *i*-th satellite will converge to some average desired relative trajectory, but in the end all of the relative deviations will decrease and the required image configuration will be obtained.

4.3 Decentralized control approach constraints

The centralized control implies the presence of a head satellite in the formation, its motion is monitored by the remaining satellites, which are controlled to achieve the required relative trajectory, or the head satellite sends the control commands to the other satellites. On the contrary, the decentralized control approach means that each satellite is controlled individually and independently based on the relative motion. It is assumed that the calculated control applied to the other satellites could be unknown.

Since in the decentralized scheme each satellite is controlled independently then the *i*-th satellite can only partially implement the calculated value. According to the aerodynamic force model $u_i^x \in [0; -u_{\max}^x]$, where $u_{\max}^i > 0$ is the absolute maximum value of $u_{ij}^x = u_j^x - u_i^x$ the acceleration.

Thus, it is assumed that in the case of the control saturation it is necessary to implement maximum possible component along the *Ox* axes, but according to the force model in this case the other components are zero: $\mathbf{u}_{\max}^x = \left[u_{\max}^x \;\; 0 \;\; 0 \right]$. In the case the calculated control $\bar{\mathbf{u}}_i$ is in the acceptable control region, then it could be implemented. But in the case if the calculated average deviation control $\bar{u}_i^x$ is of negative value, then its vector $\mathbf{u}_i$ cannot be implemented and set to zero. In the case when the $0 < \bar{u}_i^x < u_{\max}^x$ in the acceptable control region, but the sum of the other two components is saturated, i.e. $\sqrt{\left(\bar{u}_i^y\right)^2 + \left(\bar{u}_i^z\right)^2} > u_{\max}^{yz}$, then it is reasonable to implement its maximum value $u_{\max}^{yz}$. However in that case according to the Fig.4 the angle $\theta \approx 52$ deg and the *Ox* component $\tilde{u}_i^x$ at this angle is $u_i^x / k \approx 0.8$. So, the control vector to be applied in that case is $\mathbf{u}_{\max}^{yz} = \left[\tilde{u}_i^x \;\; \bar{u}_i^y / u_{\max}^{yz} \;\; \bar{u}_i^z / u_{\max}^{yz} \right]$, i.e. the calculated values for the *Oy* and *Oz* values are normalized to the maximum possible value $u_{\max}^{yz}$.

Thus, summarily, for the $\mathbf{u}_i$ one can propose the following decentralized control law:

$$\mathbf{u}_i = \begin{cases} -\mathbf{u}_{\max}^x, \text{if } \bar{u}_i^x > u_{\max}^x, \\ -\mathbf{u}_{\max}^{yz}, \text{if } 0 < \bar{u}_i^x < u_{\max}^x, \\ \qquad \text{and } \sqrt{\left(\bar{u}_i^y\right)^2 + \left(\bar{u}_i^z\right)^2} > u_{\max}^{yz}, \\ -\bar{\mathbf{u}}_i, \quad \text{if } 0 < \bar{u}_i^x < u_{\max}^x, \\ 0, \quad \text{if } \bar{u}_i^x < 0. \end{cases} \qquad (12)$$

The proposed decentralized control strategy is derived empirically based in the practical logics, its values are just partly based on the LQR because it is takes into account the aerodynamic force value constrains. So, the algorithm performance is needed to be demonstrated. Due to actual aerodynamic force restrictions the convergence of the relative deviations of the trajectories cannot be proved analytically. That is why only numerical simulations is used for the controlled motion study.

4.4 Construction of reference trajectories

To calculate the relative deviations $\mathbf{e}_{ij}$ all the reference trajectories between all the satellites should be defined. First, the required flat image has to be discretised to be represented in pixels. Next, the distance between the pixels should be set to be recognizable by human eye observing the formation in LEO. Then, such an initial velocity is defined that according to HCW free-motion equations (1) the image would rotate along closed relative orbits. To maintain the relative distances between the pixels for the observer the relative orbits are chosen as projected circular orbit. The phase of the reference orbit is calculated to provide the appropriate orientation of the image for the observer which is located in a given geographical point.

5. Numerical study

Consider the application of the proposed control rule for the problem of forming the formation after the launch. The cluster launch scheme is considered. It is assumed that the satellites separate from the launcher in the *Ox* axis direction one after another with the time interval Δt between the launches. The velocity of the ejection V_e is assumed to be the same for all the CubeSats, however due to launch system inaccuracy the ejection velocity V_e is subjected to errors. So, the initial velocity vector $\mathbf{V}_0$ in orbital reference frame is modelled as follows:

$$\mathbf{V}_0 = \begin{bmatrix} V_e + \delta V \\ \delta V \\ \delta V \end{bmatrix}, \quad (13)$$

where δV is ejection error considered as a normally distributed random value with zero mean and $\sigma_{\delta V}^2$ covariance.

After separation the implementation of control which is aimed at achieving the required formation begins. In this example, a textbox showing "IAC" is to be constructed. The reference orbits for the "IAC" construction is presented in Fig. 8. To form this image, 53 satellites are required. One can see from Fig.8 that for each satellite the reference orbit is circular.

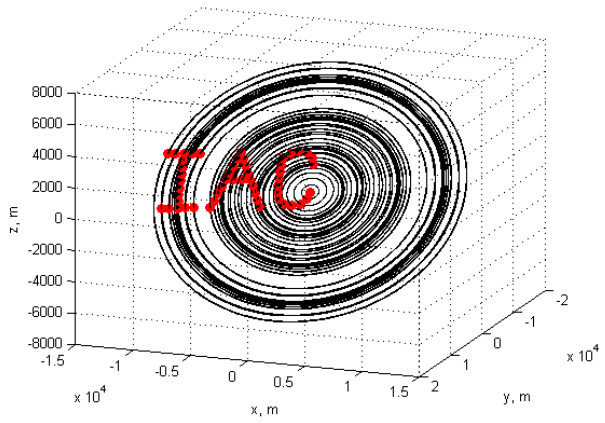

Fig.8. Reference relative orbits of the satellites

All the parameters used in the simulation of the controlled motion of the CubeSat formation are presented in Table 1. The value of the density is according to atmosphere density along the orbit with a 350 km altitude according to the Russian GOST model of upper atmosphere [21].

Table 1. Parameters of simulation

Main parameters of the formation	
Number of satellites in the formation, N	53
Distance between two the satellites in image	700 m
Launch parameters	
Time interval between the launches, Δt	10 s
Ejection velocity, V_e	0.5 m/s
Ejection error deviation, $\sigma_{\delta V}$	0.05 m/s
CubeSats parameters	
Mass of satellite, m	18 kg
Size of sunlight reflectors, S	4x4 m^2
Aerodynamic drag coefficient, C_a	2
LQR parameters	
Matrix Q	E_{6x6}
Matrix R	diag ([1e-13; 1e-14; 1e-14])
Aerodynamic drag force parameters	
Constant atmosphere density, ρ	10^{-11} kg/m^3
Orbit altitude, h	350 km
Airflow velocity, $V = \sqrt{\mu/(R_E + h)}$	7.69 km/s
Parameters ε and η	0.1
Modelling parameters	
Time of simulation, T	24 hours
Atmosphere density model	GOST model

Fig. 10 demonstrates the relative motion trajectories under the proposed decentralized control (12) relative to the last launched satellite. It can be seen that the relative trajectories converge to the desired trajectory described by free relative motion equations.

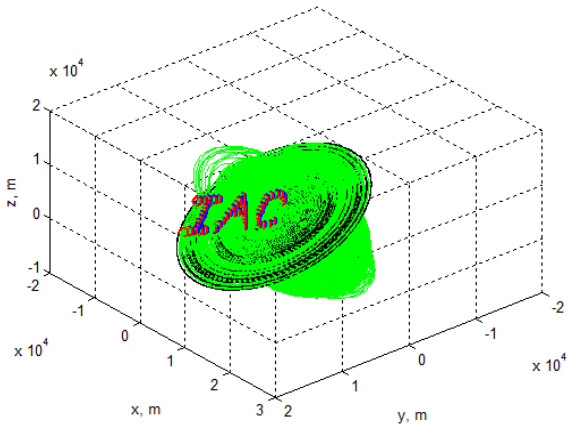

Fig. 10. Relative trajectories under the proposed control

Fig 11 shows the desired and real position of all of the satellites in the orbital reference frame after 40 hours of control. One can see that they are close to each other. Fig.11 demonstrates the deviations vector of the second-launched satellite relative to the last launched satellite. One can see that all the deviations after approximately 20 hours tend to zero. The slowest convergence is shown in the *Oy* component of the

deviation vectors due to the relatively small lift component of the aerodynamic force.

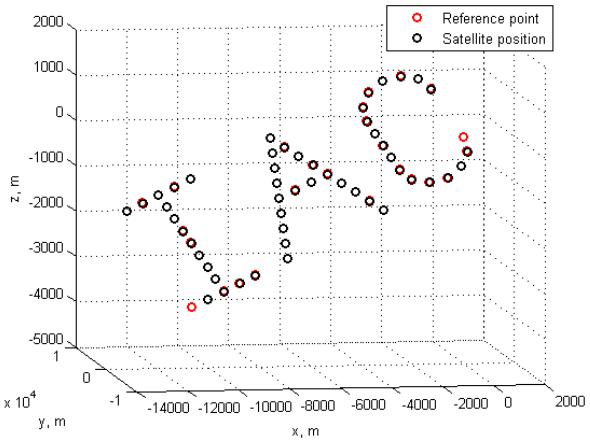

Fig. 11. Desired and real position of all of the satellite in the orbital reference frame after of 40 hours of control

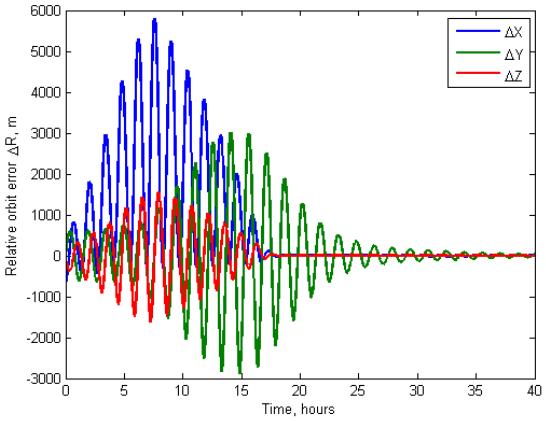

Fig. 12. Satellite position vector deviation relative to the last-launched satellite

The calculated control according to (11) for the average relative vector of deviations for the first satellite is presented in Fig. 13 as an example. The corresponding implemented value according to (12) is shown in Fig. 14. It can be seen that in the beginning the calculated value for the *Ox* component is positive. It cannot be realized by the aerodynamic force, so its value is set to zero. After approximately 3 hours the deviation along the Ox axis decreases considerably, but all the positive calculated values are still not implemented. After the 3 hours the deviation along *Oy* axis still was large enough that lead to the saturation for the corresponding control vector component. During this case that lasted about next 20 hours the second control situation from (12) was implemented. It caused a temporary increased deviation along the *Ox* axis. But after 15 hours the deviations along *Oy* axis decreased and all of the components of the calculated control came to the acceptable control region. The plots for the other satellites are similar and therefore are not presented in the paper.

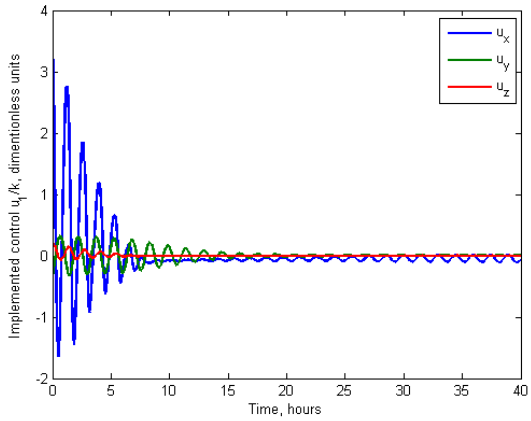

Fig. 13. Calculated control vector according to the (11) control algorithm

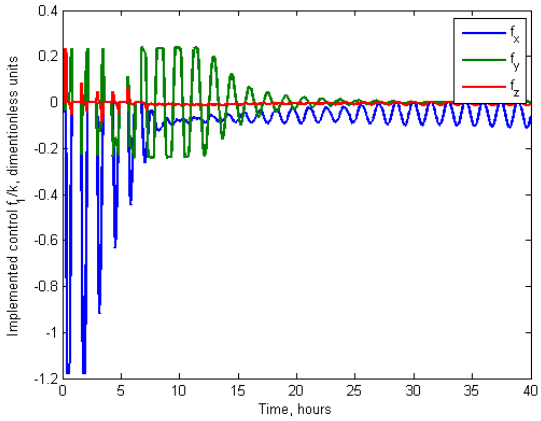

Fig. 14. The implemented control according to the (12) decentralized strategy

For the higher orbit altitude, the proposed control scheme requires more time for constructing a flat image. The slowest is y-component error vector because it is controlled by the lift force which is about 10 times smaller than the aerodynamic drag. The convergence time for the out-of-plane relative component can take several days, which is unacceptable. So, for the orbits with altitude of 400km and more thruster actuation should be considered to obtain faster image construction in out-of-plane direction.

6. Conclusions

The decentralized control scheme is proposed for constructing a formation showing a flat image using the aerodynamic force with the lift component. Its application is demonstrated using 53 satellites with sunlight reflectors. The preliminary study shows that for such satellites under appropriate illumination conditions it is possible to observe the satellites as a defined image

from the ground. Considering acceptable time for image construction of about several hours it is shown that fully aerodynamic control can be applied only for the orbits with altitudes of 400 km and lower.

Acknowledgements

The work supported by Russian Foundation for Basic Research, grant № 17-01-00449_a.

References

[1] C.L. Leonard, Formation Keeping of Spacecraft via Differential Drag, Master Thesis, Massachusetts Inst. Technol. (1986).

[2] B.S. Kumar, A. Ng, A. Bang-Bang, Control Approach to Maneuver Spacecraft in a Formation With Differential Drag, in: Proc. AIAA Guid. Navig. Control Conf. Exhib. AIAA Pap. No.2008-6469, Honolulu, Hawaii, August 2008., n.d.

[3] D. Ivanov, M. Kushniruk, M. Ovchinnikov, Study of satellite formation flying control using differential lift and drag, Acta Astronaut. 145 (2018) 88–100. doi:10.1016/J.ACTAASTRO.2018.07.047.

[4] D. Pérez, R. Bevilacqua, Lyapunov-Based Adaptive Feedback for Spacecraft Planar Relative Maneuvering via Differential Drag, J. Guid. Control. Dyn. 37 (2014) 1678–1684. doi:10.2514/1.G000191.

[5] D. Pérez, R. Bevilacqua, Differential drag spacecraft rendezvous using an adaptive Lyapunov control strategy, Acta Astronaut. 83 (2013) 196–207. doi:10.1016/j.actaastro.2012.09.005.

[6] K.D. Kumar, A.K. Misra, S. Varma, F. Bellefeuille, Maintenance of Satellite Formations Using Environmental Forces, Acta Astronaut. 102 (2014) 341–354. doi:10.1016/j.actaastro.2014.05.001.

[7] L. Dellelce, G. Kerschen, Optimal propellantless rendez-vous using differential drag, Acta Astronaut. 109 (2015) 112–123. doi:10.1016/j.actaastro.2015.01.011.

[8] O. Ben-Yaacov, P. Gurfil, Long-Term Cluster Flight of Multiple Satellites Using Differential Drag, J. Guid. Control. Dyn. 36 (2013) 1731–1740. doi:10.2514/1.61496.

[9] O. Ben-Yaacov, P. Gurfil, Orbital elements feedback for cluster keeping using differential drag, Adv. Astronaut. Sci. 153 (2015) 769–787. doi:10.1007/s40295-014-0022-0.

[10] M. Horsley, S. Nikolaev, A. Pertica, Small Satellite Rendezvous Using Differential Lift and Drag, J. Guid. Control. Dyn. 36 (2013) 445–453. doi:10.2514/1.57327.

[11] L.H. Sentman, Comparison of the Exact and Approximate Methods for Predicting Free Molecule Aerodynamic Coefficients, ARS J. 31 (1961) 1567–1579.

[12] B. Smith, R. Boyce, L. Brown, M. Garratt, Investigation into the Practicability of Differential Lift-Based Spacecraft Rendezvous, J. Guid. Control. Dyn. 40 (2017) 2680–2687. doi:10.2514/1.G002537.

[13] R. Sun, J. Wang, D. Zhang, Q. Jia, X. Shao, Neural-Network-Based Sliding-Mode Adaptive Control for Spacecraft Formation Using Aerodynamic Forces, J. Guid. Control. Dyn. (2017) 1–13. doi:10.2514/1.G003130.

[14] R. Sun, J. Wang, D. Zhang, X. Shao, Neural network-based sliding mode control for atmospheric-actuated spacecraft formation using switching strategy, Adv. Sp. Res. (2017) 1–13. doi:10.1016/j.asr.2017.11.011.

[15] X. Shao, M. Song, J. Wang, D. Zhang, J. Chen, Satellite formation keeping using differential lift and drag under J2 perturbation, Aircr. Eng. Aerosp. Technol. 89 (2017) 11–19.

[16] S. Biktimirov, A. Ivanov, A. Kharlan, N. Mullin, D. Pritykin, Deployment and maintenance of solar sail-equipped CubeSat formation in LEO, in: 18th Aust. Int. Aerosp. Congr. ISSFD - 27th Int. Symp. Sp. Flight Dyn. (ISSFD). Melb. Eng. Aust. R. Aeronaut. Soc., 2019: pp. 983–988.

[17] G.W. Hill, Researches in Lunar Theory, Am. J. Math. 1 (1878) 5–26.

[18] Schweighart S.; Sedwick R.J., High-Fidelity Linearized J2 Model for Satellite Formation Flight, J. Guid. Control. Dyn. 25 (2002) 1073–1080.

[19] V.V. Beletsky, A.M. Yanshin, Influence of Aerodynamic Forces on Satellites Attitude Motion, Naukova Dumka, Kiev, 1984.

[20] M. Ciarci, A. Grompone, M. Romano, A near-optimal guidance for cooperative docking maneuvers, Acta Astronaut. 102 (2014) 367–377. doi:10.1016/j.actaastro.2014.01.002.

[21] D.A. Vallado, ed., Fundamentals of Astrodynamics and Applications, 2nd ed., Microcosm, Inc, El Segundo, 2001.